Graphene-based Frequency Selective Surface Decoupling Structure for Ultra-dense Multi-band Plasmonic Nano-antenna Arrays

Bin Zhang
Wuhan University of Technology
Georgia Institute of Technology
xttzhb@whut.edu.cn

Josep M. Jornet
University at Buffalo
Buffalo, NY, USA
jmjornet@buffalo.edu

Ian F. Akyildiz
Georgia Institute of Technology
Atlanta, GA, USA
ian@ece.gatech.edu

Zhi P. Wu
Wuhan University of Technology
Wuhan, China
z.p.wu@whut.edu.cn

ABSTRACT

A four-layer graphene-based frequency selective surface (FSS) is proposed to reduce the mutual coupling in ultra-dense plasmonic nano-antenna arrays for multi-band Ultra-Massive MIMO communications. In the proposed structure, graphene is utilized as a cross patch FSS, which is low-profile and tunable. The FSS structure shows a wide stop-band (-15 dB) from 1.1 THz to 1.7 THz. By inserting the FSS structure between the elements of the nano-antenna array, a high isolation of -25 dB with a 15 dB fall is achieved, which indicates that mutual decoupling effects are suppressed for both two-element and four-element arrays. The radiation patterns are given to confirm that the proposed FSS structure can improve the performance of multi-band THz antenna arrays with negligible influence on the nano-antenna radiation performance. Finally, it is asymptotically shown that the mutual coupling experienced by the nano-antenna with the FSS structure is negligible even in the presence of very large number of closely integrated elements.

CCS CONCEPTS

• **Hardware → Wireless devices**;

KEYWORDS

Graphene, decoupling, FSS, multi-band, UM MIMO, Terahertz Communications

ACM Reference Format:
Bin Zhang, Josep M. Jornet, Ian F. Akyildiz, and Zhi P. Wu. 2018. Graphene-based Frequency Selective Surface Decoupling Structure for Ultra-dense Multi-band Plasmonic Nano-antenna Arrays . In *NANOCOM '18: NANOCOM '18: ACM The Fifth Annual International Conference on Nanoscale Computing and Communication, September 5–7, 2018, Reykjavik, Iceland.* ACM, New York, NY, USA, 6 pages. https://doi.org/10.1145/3233188.3233211

NANOCOM '18, September 5–7, 2018, Reykjavik, Iceland

ACM ISBN 978-1-4503-5711-1/18/09…$15.00
https://doi.org/10.1145/3233188.3233211

1 INTRODUCTION

With the increasing demand for faster data rates in recent years, the Terahertz band (0.1-10 THz) has been envisioned as one of the promising spectrum regions to enable Terabit-per-second (Tbps) links required in future generation communication systems [1]. In the THz band, the available transmission bandwidth drastically changes with the distance and the medium molecular composition [2]. For short distances, the THz band behaves as a single transmission window with almost 10 THz bandwidth, whilst for long distances, molecular absorption delimits several transmission windows, tens to hundreds of GHz each. However, the huge bandwidth of THz band comes with a high propagation loss in free space, which combined with the low output power of THz sources, limit the communication distance. To overcome this limitation, the utilization of very dense nano-antenna arrays in Ultra-massive (UM) MIMO communication systems has been recently proposed [3]. Besides beamforming and spatial multiplexing, to maximize the utilization of the THz band, the concept of multi-band UM MIMO has been introduced. This technique is enabled by leveraging the tunability of novel graphene-based plasmonic devices.

Graphene, a two-dimensional material with unprecedented electrical and optical properties [4], is an enabling material for the realization of very dense nano-antenna arrays. Compared with metals, graphene exhibits a unique frequency-dependent complex-valued conductivity which enables the propagation of Surface Plasmon Polariton (SPP) waves at THz-band frequencies [5]. SPP waves are surface-confined EM waves that result from the global oscillations of electrons on the graphene layer. The propagation speed of SPP waves is much lower than that of free-space EM waves, and, as a result, graphene-based plasmonic devices at THz frequencies are up to two orders smaller than their metallic counterparts. Among others, this feature has led to the integration of graphene-based plasmonic nano-antennas in very small footprints. Since the first work on graphene-based nano-antennas in 2010 [6], many aspects of graphene-based nano-antennas have been explored. For example, it has been shown that the resonant frequency of the graphene-based plasmonic nano-antenna can be electrically tuned [7]. As a result, nano-antenna arrays able to simultaneously operate at different resonant frequencies can be realized.

In such very dense nano-antenna array structures, mutual coupling between elements can drastically impact the array performance and ultimately limit the communication distance. Mutual coupling effects are generally caused by radiation in free space as well as surface wave interactions from adjacent antenna elements [8]. For planar graphene-based nano-antennas, the coupling effects are mainly from surface waves and their near-field radiation. Strong coupling effects would result in high correlation and low isolation between elements [9]. It is important to note that graphene demonstrates natural advantages on reduction of mutual coupling effects because of the short SPP wavelength resulting from the slow propagation speed of SPP waves. In this way, graphene-based antennas exhibit lower mutual coupling effects than metal antenna arrays with the same distance between elements [10].

Nevertheless, the residual contributions to the total coupling from massive numbers of neighboring antennas requires the development of decoupling techniques [11–13]. Existing works mainly rely on the use of metallic structures, which introduce high losses and can be challenging to integrate with graphene structures. Therefore, it is desired to again use graphene for the decoupling structure. Moreover, the tunability of graphene can be exploited to create broadband decoupling structures. For example, in [14], a graphene cloak is used to reduce the coupling effects between two dipole antennas. While the use of graphene in decoupling structures has been suggested in the related literature [15], the benefits introduced by its tunability have not been neither discussed nor exploited.

In this paper, we design and propose the utilization of a graphene-based Frequency Selective Surface (FSS) decoupling structure to reduce the coupling effects of multi-band UM MIMO arrays. More specifically, first, we present the FSS design and we analytically model and numerically simulate it. Then, we investigate the performance of ultra-massive nano-antenna systems when the FSS structure is embedded in the array. Our results show that the FSS can successfully reduce the coupling by a factor of 15 dB while not changing the antenna array radiation diagram. An asymptotically analysis confirms coupling effects between ultra-massive nano-antenna arrays are negligible with FSS in presence.

The rest of the paper is organized as follows. A dual-band antenna array prototype model is presented and the mutual coupling effects of this model are investigated in Section 2. The graphene-based FSS decoupling structure is proposed and analyzed in Section 3. Implanting the FSS structure between the antenna arrays, the performances of the arrays with FSS structures are investigated and results are discussed in Section 4. Finally, conclusions are drawn in Section 5.

2 ANTENNA ARRAY DESIGN AND MUTUAL COUPLING EFFECTS

In this section, we present the design of the graphene-based nano-antenna array considered in our analysis. First, the complex conductivity model of graphene and the dispersion relationship for SPP waves are recalled and the design and analysis of graphene-based nano-antenna array is conducted. Then, the mutual coupling effects between adjacent nano-antennas are investigated. Several parameters are presented to evaluate the impact of coupling effects.

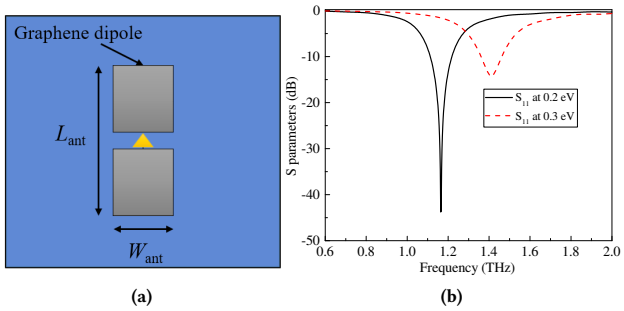

(a) (b)

Figure 1: Graphene-based plasmonic nano-antenna. (a) Schematic diagram and (b) return loss of antenna being tuned with different chemical potential levels.

2.1 Graphene-based Plasmonic Nano-antenna Design

The proposed multi-band nano-antenna array consists of several sub-sets of nano-antennas working at different frequency bands. There are different types of the sub-array schemes, which require the antenna elements to be capable to switch from one working band to other bands. Thus, the basic element of the sub-array should be frequency reconfigurable. This is achieved by leveraging the frequency-tunability of graphene.

The surface conductivity of graphene is described by using the Kubo formula and is a function of frequency $f = \omega/2\pi$, Fermi energy E_F and relaxation time τ. The total conductivity is given by [5]

$$\sigma^g = \sigma^g_{intra} + \sigma^g_{inter} \tag{1}$$

$$\sigma^g_{inter} = \frac{2e^2 k_B T}{\pi\hbar^2} \ln\left(2\cosh\left(\frac{E_F}{2k_B T}\right)\right) \frac{i}{\omega + i\tau^{-1}}, \tag{2}$$

$$\sigma^g_{inter} = \frac{e^2}{4\hbar}\left(H\left(\frac{\omega}{2}\right) + i\frac{4\omega}{\pi}\int_0^\infty \frac{H(\Xi) - H(\omega/2)}{\omega^2 - 4\Xi^2} d\Xi\right), \tag{3}$$

and

$$H(a) = \frac{\sinh(\hbar a/k_B T)}{cosh(E_F/k_B T) + \cosh(\hbar a/k_B T)}, \tag{4}$$

where $\hbar = h/2\pi$ is the normalized Planck's constant, e is the electron charge, k_B is the Boltzmann constant and T stands for temperature. The conductivity can easily be tuned by applying a bias voltage or chemical doping. The propagation of TM SPP waves follows the simplified dispersion relationship below [16]

$$-i\frac{\sigma_g}{\omega\varepsilon_0} = \frac{\varepsilon_1 + \varepsilon_2}{k_{spp}}, \tag{5}$$

where ε_1 and ε_2 denote the permittivity of media above and beneath graphene sheet. k_{spp} is the complex propagation constant of TM SPP waves. The SPP wavelength is given by $\lambda_{spp} = 2\pi/\mathrm{Re}\left[k_{spp}\right]$. By changing the Fermi energy, the conductivity is dynamically tuned, then the antenna based on graphene becomes frequency reconfigurable.

In Figure 1a, we illustrate the reference antenna design that we utilize in this paper. For convenience, a dipole patch antenna is employed as the basic antenna element. The dipole patches made with single layer graphene are paved on a quartz (SiO_2) substrate.

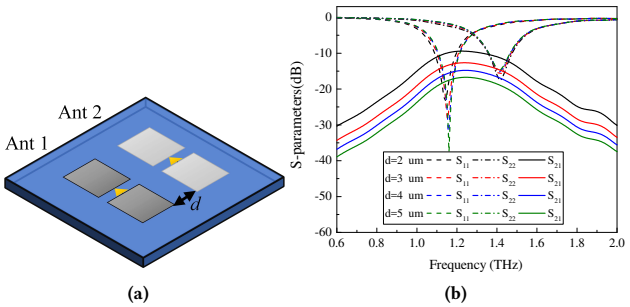

Figure 2: Dual-band two-element graphene-based antenna array with separation distance of 2 μm. (a) Schematic diagram and (b) simulated S-parameter curves.

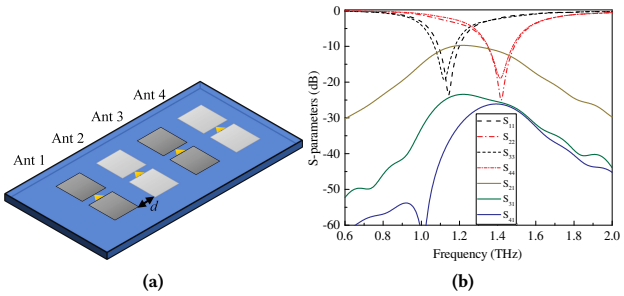

Figure 3: Dual-band four-element graphene-based antenna array with separation distance of 2 μm. (a) Schematic diagram and (b) simulated S-parameter curves.

The graphene-based patch is defined by length L_{ant} = 11 μm and width W_{ant} = 5 μm. The gap between the two arms is 1 μm. A photoconductive source or a graphene-gated HEMT source is the potential way to feed the antenna. The frequency response of the antenna is reconfigurable with respect to biasing or chemical doping. The simulation of the antenna is conducted by using the full-wave analysis software CST Microwave Studio. Figure 1b gives the reflection coefficients S_{11} of the antenna while the chemical potential is set as 0.2 eV and 0.3 eV, respectively. One can observe that the graphene-based plasmonic nano-antenna with fixed physical dimensions demonstrates multi-band property while the antenna is tuned at different Fermi energy levels.

2.2 Mutual Coupling Between Adjacent Nano-antennas

In multi-band UM MIMO systems, there are thousands of antenna elements, but the dominant mutual coupling effects usually exist between the adjacent elements in most cases. Here, we consider two different cases: dual-band two-element and dual-band four-element linear arrays. In the first case, two antennas, Antenna 1 and Antenna 2, with the same dimensions but being tuned with energy levels 0.2 eV and 0.3 eV are placed within a certain distance, as shown in Figure 2a. For the array with four elements, the two antennas are linearly interleaved with a uniform space between them, as shown in Figure 3a. The N-antenna array is seen as a N-port system. We use the transmission coefficient between two ports to describe the mutual coupling effects of the system. There are several parameters to describe the mutual coupling effects for the two-element array. Among them, the scattering parameter S_{21}, i.e., the isolation coefficient, is a basic form to evaluate the effects. The isolation coefficients with various distances between antenna elements are analyzed for both cases.

For the two-element case, the isolation parameters, i.e., S_{21} coefficients, are obtained between two elements separated by an edge-to-edge distance ranging from 2 to 4 μm. The results show that at distance of 2 μm, which is about one fifth of the SPP wavelength and the peak value of the S_{21} curve is approximately -9.4 dB, which is not acceptable for an array system. As the distance rises, the isolation between two elements decreases to -17 dB, as shown in Figure 2b. For the array with four antennas, we choose Antenna 1 as object of study and present S_{21}, S_{31}, S_{41} to show the influence from the other elements. In Figure 3b, we can see that S_{31} and S_{41} give a low peak of -25 dB, which is negligible compared with S_{21}. We only need to tackle the problem of isolation between the two adjacent elements. These S_{21} values are insufficient due to the low efficiency and sophistication for THz multi-band UM MIMO systems. Thus, there would have potential to reduce the mutual coupling by using decoupling structure like FSS but not increasing the space between antenna elements at the same time.

The antenna radiation pattern, i.e., the power radiated by antenna as a function of space coordinates, is another significant feature that is affected by mutual coupling effects. Especially in antenna arrays, the far-field radiation pattern is strongly based on the pattern of a single element. In the following sections, the radiation pattern is also presented to evaluate the decoupling effects.

3 GRAPHENE-BASED FSS DESIGN

A frequency selective surface structure is a periodic patch or slot structure with band stop or band pass characteristics. To some extent, a FSS behaves as a spatial filter. For band-stop purpose, patch-based FSSs are employed in this case. A unit cell is the most basic structure of FSS. The performance of a full-dimension FSS structure is achieved by extending the unit cell result with Floquet's principle [17]. Commonly, the wavelength of resonance is calculated approximately as twice the element length by $L_{FSS} \simeq \lambda_c/2$ [17]. However, in a practical way, the element length is not exactly half wavelength due to the substrate effect and dispersive nature of SPP waves on graphene. The working frequency of the FSS is determined by the element length, substrate permittivity and substrate dimensions. Among them, the patch length is the significant one can directly influence the working frequency of the FSS structure. Also, the width of element is usually much smaller than the length.

Here, we propose a graphene-based cross patch FSS structure working at THz frequencies. For multi-band and reconfigurable purpose, graphene becomes a reasonable choice to be employed as patch materials in FSS structure. We can achieve multi-band with one fixed-size FSS patch/slot by simply modifying the chemical potential level. In this case, a cross patch is selected as the unit cell element for its cross-polarization character, with arm length L_{cross} = 10.97 μm and width W_{cross} = 3 μm. The length of the

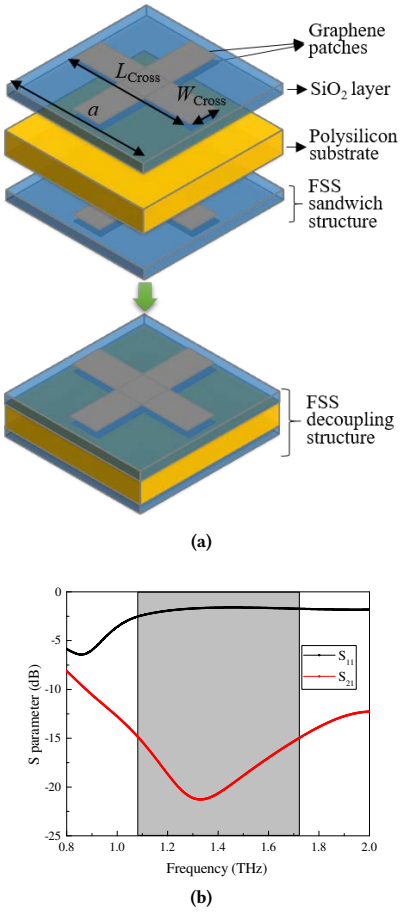

Figure 4: The proposed FSS decoupling structure for multi-band array: (a) Configuration diagram and (b) simulated S-parameters results. Grey area is the -15 dB bandwidth.

square substrate is a = 11 μm. In Figure 4a, the schematic of the proposed FSS structure is presented. For better resonance and wider working band, four layers of graphene-based cross patches are used in the design of the FSS. Two single-layer graphene cross patches with the same energy level and one SiO_2 film (thickness is 0.2 μm) between the patches compose a FSS sandwich structure. There are two sandwich structures attached on each side of a 0.6-μm-thick polysilicon substrate with permittivity of 11.9. For multi-band UM MIMO system, the Fermi energy level should be chosen carefully to make the FSS patch resonate at the working bands of the aforementioned antenna array. Here, we set 0.2 eV and 0.3 eV as graphene chemical potential for each sandwich structure to cover the working frequency bands of both antennas presented in the previous section. Temperature of graphene is set as 300 K and the relaxation time is 0.5 ps. It should be noted that due to the coupling effects between the FSS patches the working band of the structure is not simply the combination of two resonant frequencies of FSS at 0.2 eV and 0.3 eV. Also, the distance between the patches is too small that the two patches in the same sandwich structure are strongly

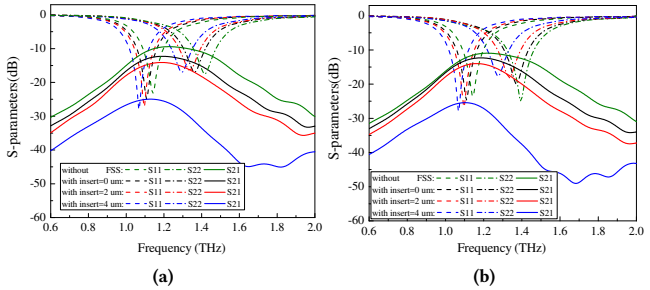

Figure 5: S-parameters versus frequency of (a) two-element case and (b) four-element case.

coupled as a capacity, which leads to a frequency shift of the FSS structure.

The full wave performance analysis of the FSS structures is carried out by CST Microwave Studio. A planar wave is used as input signal to get the frequency response of the structure. Noted that only normal incidence is considered in the simulation. The simulated performances of the FSS are given in Figure 4. It is observed that the proposed FSS decoupling structure has a wide -15 dB bandwidth from 1.1 THz to 1.7 THz. The -10 dB bandwidth is more than 1 THz starting from 0.9 THz, which efficiently covers both target frequency ranges: 1.1 THz-1.25 THz and 1.35 THz-1.5 THz. Furthermore, we can utilize this FSS structure to cover other frequency ranges by properly modifying the energy levels of graphene patches. The proposed FSS structure shows the potential to be employed for reduction of coupling effects of the proposed antenna array or even any other antenna arrays with different working bands.

4 PERFORMANCE ANALYSIS AND DISCUSSION

In order to reduce the mutual coupling effects, the proposed structure is mounted between the two adjacent antenna elements with separation distance of 2 μm. The magnitude of the isolation with separation distance of 2 μm presented in Section 2 is approximately -10 dB, which is not acceptable and can certainly be improved. What is more, due to the high substrate permittivity, the SPP wave energy is mostly guided backward and part of the energy is stored and transmitted in the substrate. In this context, we propose to insert FSS decoupling structure into the substrate of the nano-antenna array to block the wave propagation between the elements. Moreover, it is practically feasible to insert a FSS structure into a dielectric substrate. Here, we consider both two-element and four-element arrays to study the decoupling performance of FSS structures. The edge-to-edge distance between the two adjacent elements is set as 2 μm, which is approximately one fifth of the SPP wavelength. Then, the asymptotic behavior in massive multi-band arrays is evaluated.

4.1 Multi-band Graphene-based Array with Two and Four Elements

The two-element and four-element nano-antenna arrays with FSS decoupling structures are simulated in CST Microwave Studio. The minimum mesh cell is defined as 0.15 μm for accuracy, which

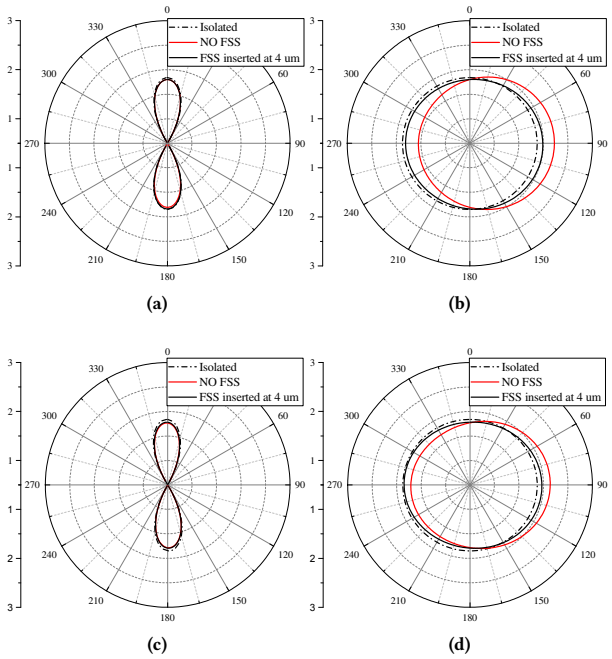

Figure 6: Radiation patterns of Antenna 1 in both arrays: (a) E-plane and (b) H-plane for two-element case, (c) E-plane and (d) H-plane for four-element case.

is far smaller than the SPP wavelength. Besides the standard S-parameters, a far-field monitor is used to observe the radiation performance. Also, an open boundary condition is employed to study the far-field distribution.

In Figure 5, the S-parameters are illustrated for four scenarios: nano-antenna array without FSS structure, nano-antenna array with FSS structure mounted between elements and nano-antenna array with FSS structure inserted into substrate with insertion depth of 2 and 4 μm. It is clearly seen that there is a maximum 5 dB drop of isolation coefficient after using the proposed FSS structure. With insert depth rises from 0 to 4 μm, the max isolation decreases from the original -9.4 dB to approximately -25 dB, which is more than a 15 dB drop. Similar results are obtained in the four-element case, as shown in Figure 5b. It should be noted that using FSS structures in nano-antenna array systems also lead to a resonant frequency shift of 8.5% compared to the original nano-antenna resonant frequencies, as shown in Figure 5. This is a result from the coupling between the antenna element and FSS structure.

The radiation pattern can also be strongly affected due to the coupling between antenna elements. Figure 6 shows the radiation patterns of Antenna 1 at the targeted working frequency. Three cases are considered to validate the reduction of mutual coupling effects because of the FSS decoupling structure: an isolated antenna, an antenna in array without FSS and an antenna in array with FSS. Particularly, both the E-plane and H-plane patterns are given. In Figure 6a, the E-plane is slightly influenced due to the arrangement of the array elements. However, the coupling between the elements would strongly affect the H-plane of the radiation pattern, as shown

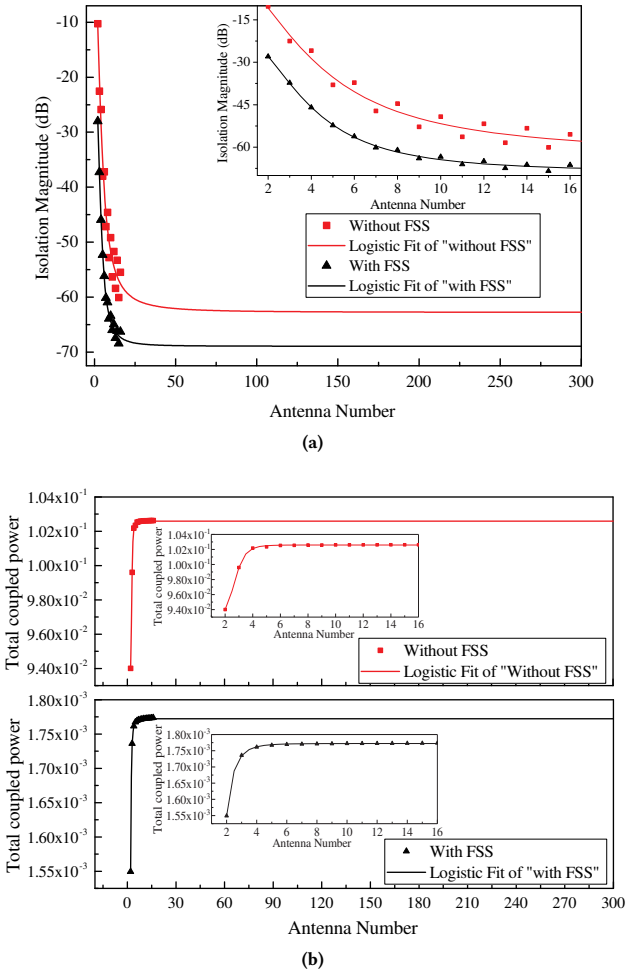

Figure 7: Asymptotic results over different antenna numbers. (a) Magnitude of isolation coefficient data and fitted curves. (b) Total coupled power results and fitted curve over antenna number.

in Figure 6b. After inserting of the FSS structure, both radiation patterns are recovered well as if antennas are originally isolated without coupling. For the four-element array, radiation patterns of Antenna 1 is given and well restored in Figure 6c and 6d. The results reveal the coupling effects have negligible influence on E-plane radiation pattern of antenna and FSS structure can efficiently recover the H-plane pattern for the antenna elements.

4.2 Asymptotic Behavior in Massive Multi-band Arrays

To evaluate the performance of the proposed FSS structures when the antenna number increases to infinity, isolation coefficients of a linear array with 16 elements are simulated and analyzed. Then the asymptotic behavior of the ultra-massive multi-band array is foretold by using curve fitting technique.

In this case, the two antennas with different working bands are interleaved along one direction and the FSS structures are placed in between the antennas. Figure 7 plots the magnitudes of isolation coefficients between Antenna 1 and Antenna N. Two cases are considered in this plot, the array with and without decoupling structures. A curve fitting technique based on Logistic function is employed to show the trend. We can observe that the isolation coefficients between the elements plunge with the increasing of antenna number from 2 to 25. Then the curve decreases with lower bound of -63 dB when antenna number increases from 2 to 300. It is predictable the magnitudes of the isolations would fall gently and verge to a constant according the fitted curves. It is worth noting that there is regularly fluctuation of the magnitude values, which is resulted from the interleave arrangement of the array. With the FSS structures mounted in array, the trend declines drastically and ends up with a lower bound of -68 dB, which is smaller than the curve in the case that without FSS. This confirms that the FSS structures work well with decoupling and the coupling effects between distant elements are insignificant.

Moreover, the total effects on Antenna 1 from other antennas are calculated and analyzed. In detail, we sum up all isolation coefficients cumulatively between Antenna 1 and Antenna N. The isolation coefficient S_{NM} denotes the power ratio from port N to M due to the reciprocity of S-parameters. Consider an array with uniform excitation power P_0 at each antenna port, isolation between Antenna 1 and Antenna N is

$$S_{N1}(dB) = 10\lg(|S_{N1}|) = 10\lg\left(\frac{P_N}{P_0}\right), \tag{6}$$

where $S_{N1}(dB)$ is the isolation in dB and $|S_{N1}|$ is the linear value of the isolation coefficient. P_N denotes the coupled power from Antenna N to Antenna 1. Set P_0 as 1, then the total coupled power on Antenna 1 is written as

$$P_{total} = \sum_{i=2}^{N} P_i = \sum_{i=2}^{N} |S_{i1}|^2. \tag{7}$$

In this way, we obtain the total influence on Antenna 1 from all neighboring antennas when the number of array elements increases.

In Figure 7b, the total coupled power is presented for two cases, before and after employing FSS structures in array. The enlarged views of the original data are plotted as well in insets. The results indicate the coupled power verges to a constant when the antenna number increases. The asymptotic total power percentage from neighboring antenna elements is 0.102 and 0.00177 with and without FSS decoupling structures, respectively. It is also observed from the inset figures that the total coupled energy verges to a constant at the antenna number of 6, which validates the dominating coupling effects are mainly from neighboring and near distance elements. With the FSS decoupling structure in place, one can forecast that the total coupled power from all other elements in one array would verge to a very small constant, compared to the case without FSS, when antenna number increases to infinity. Furthermore, the graphene-based FSS structure can cover the transmission band of interest by properly tunning the Fermi energy level, which suggests the proposed FSS decoupling structure is able to handle the arrays with increasing number of working bands at the same time.

5 CONCLUSIONS

In this paper, a graphene-based FSS structure has been integrated in a dual-band UM MIMO antenna array to reduce the mutual coupling effects between the elements. The isolation of the UM MIMO array was further improved by inserting the FSS decoupling structure into the substrate to block the electromagnetic wave propagation in the substrate. Moreover, radiation performances of the nano-antennas are insignificantly influenced with FSS in place. Although this structure has been designed for a dual-band UM MIMO array, we can extend the working band of the structure by adjusting the energy levels of graphene patches to other desired frequencies.

ACKNOWLEDGMENTS

This work was supported by China Scholarship Council.

REFERENCES

[1] Ian F. Akyildiz, Josep M. Jornet, and Chong Han. Terahertz band: Next frontier for wireless communications. *Physical Communication*, 12:16–32, 2014.
[2] Josep M. Jornet and Ian F. Akyildiz. Channel modeling and capacity analysis for electromagnetic wireless nanonetworks in the terahertz band. *IEEE Transactions on Wireless Communications*, 10(10):3211–3221, 2011.
[3] Ian F. Akyildiz and Josep M. Jornet. Realizing Ultra-Massive MIMO (1024×1024) communication in the (0.06-10) Terahertz band. *Nano Communication Networks*, 8:46–54, 2016.
[4] Andre K. Geim and Konstantin S. Novoselov. The rise of graphene. *Nature materials*, 6(3):183–191, 2007.
[5] George W. Hanson. Dyadic Green's functions and guided surface waves for a surface conductivity model of graphene. *Journal of Applied Physics*, 103(6):064302, 2008.
[6] Josep M. Jornet and Ian F. Akyildiz. Graphene-Based Nano-Antennas for Electromagnetic Nanocommunications in the Terahertz Band. In *Proceedings of the Fourth European Conference on Antennas and Propagation (EuCAP)*, pages 1–5. IEEE, Barcelona, Spain, 2010.
[7] Ignacio Llatser, Christian Kremers, Albert Cabellos-Aparicio, Josep M. Jornet, Eduard Alarcón, and Dmitry N. Chigrin. Graphene-based nano-patch antenna for terahertz radiation. *Photonics and Nanostructures - Fundamentals and Applications*, 10(4):353–358, oct 2012.
[8] Zeeshan Qamar, Umair Naeem, and Shahid A Khan. Mutual Coupling Reduction for High Performance Densely Packed Patch Antenna Arrays on Finite Substrate. *IEEE Transactions on Antennas and Propagation*, 64(5):1653–1660, 2016.
[9] Mohammad S. Sharawi. Printed multi-band MIMO Antenna Systems and Their Performance Metrics. *IEEE Antennas and Propagation Magazine*, 55(5):218–232, 2013.
[10] Luke Zakrajsek, Erik Einarsson, Ngwe Thawdar, and Josep M. Jornet. Design of graphene-based plasmonic nano-antenna arrays in the presence of mutual coupling. In *Proc. of the 11th European Conference on Antennas and Propagation*, pages 1381–1385. Paris, France, 2017.
[11] Kun Wei, Jian Ying Li, Ling Wang, Zi Jian Xing, and Rui Xu. Mutual Coupling Reduction by Novel Fractal Defected Ground Structure Bandgap Filter. *IEEE Transactions on Antennas and Propagation*, 64(10):4328–4335, 2016.
[12] Xin Mi Yang, Xue Guan Liu, Xiao Yang Zhou, and Tie Jun Cui. Reduction of Mutual Coupling Between Closely Packed Patch Antennas Using Waveguided Metamaterials. *IEEE Antennas and Wireless Propagation Letters*, 11:389–391, 2012.
[13] Reza Karimian, Arun Kesavan, Mourad Nedil, and Tayeb A Denidni. Low-Mutual-Coupling 60-GHz MIMO Antenna System With Frequency Selective Surface Wall. *IEEE Antennas and Wireless Propagation Letters*, 16:373–376, 2017.
[14] Gabriel Moreno, Hossein M. Bernety, and Alexander B. Yakovlev. Reduction of mutual coupling between strip dipole antennas at terahertz frequencies with an elliptically shaped graphene monolayer. In *2016 IEEE International Symposium on Antennas and Propagation (APSURSI)*, pages 887–888. IEEE, jun 2016.
[15] Jeet Ghosh and Debasis Mitra. Mutual coupling reduction in planar antenna by graphene metasurface for THz application. *Journal of Electromagnetic Waves and Applications*, 31(18):2036–2045, dec 2017.
[16] Marinko Jablan, Hrvoje Buljan, and Marin Soljačić. Plasmonics in graphene at infrared frequencies. *Physical Review B*, 80(24):245435, dec 2009.
[17] John C Vardaxoglou. *Frequency selective surfaces: analysis and design.* Research Studies Press , Wiley, 1997.